The Astrophysical Journal, 748:78 (14pp), 2012 April 1 doi:10.1088/0004-637X/748/2/78

MAPPING GROWTH AND GRAVITY WITH ROBUST REDSHIFT SPACE DISTORTIONS

Juliana Kwan[1,2], Geraint F. Lewis[1], and Eric V. Linder[3,4]
[1] Sydney Institute for Astronomy, School of Physics, A28, The University of Sydney, NSW 2006, Australia
[2] High Energy Physics Division, Argonne National Laboratory, Lemont, IL 60439, USA
[3] Berkeley Lab, University of California, Berkeley, CA 94720, USA
[4] Institute for the Early Universe WCU, Ewha Womans University, Seoul, Republic of Korea
Received 2011 August 14; accepted 2012 January 16; published 2012 March 9

ABSTRACT

Redshift space distortions (RSDs) caused by galaxy peculiar velocities provide a window onto the growth rate of large-scale structure and a method for testing general relativity. We investigate through a comparison of *N*-body simulations to various extensions of perturbation theory beyond the linear regime, the robustness of cosmological parameter extraction, including the gravitational growth index γ. We find that the Kaiser formula and some perturbation theory approaches bias the growth rate by 1σ or more relative to the fiducial at scales as large as $k > 0.07\,h$ Mpc^{-1}. This bias propagates to estimates of the gravitational growth index as well as Ω_m and the equation-of-state parameter and presents a significant challenge to modeling RSDs. We also determine an accurate fitting function for a combination of line-of-sight damping and higher order angular dependence that allows robust modeling of the redshift space power spectrum to substantially higher k.

Key words: cosmological parameters – cosmology: theory – large-scale structure of Universe

Online-only material: color figures

1. INTRODUCTION

Large-scale structure surveys provide key pieces of evidence for the accelerated expansion of the universe and historically have made substantial contributions to establish Λ-cold dark matter (ΛCDM) as the current standard model of cosmology. Measurements of the baryon acoustic oscillation (BAO) scale and the shape of the matter power spectrum continue to be essential probes of cosmology. But although the amount of cosmological data grows, the presence of a cosmological constant Λ, or other forms of dark energy, has yet to be confirmed by observations over much of cosmic time (from $1 < z < 1100$) and some highly undesirable features of ΛCDM, such as the cosmic coincidence problem and a discrepancy of 120 orders of magnitude in the value of Λ (Carroll 2001), are still unsolved.

A possible alternative explanation of cosmic acceleration suggests that the nature of gravity deviates from general relativity on large scales, thus affecting the measurement of the distance–redshift relation and the manner in which large-scale structure forms. Recently, the redshift space distortions (RSDs) seen in large-scale structure surveys have emerged as a powerful new method of probing such a gravitational origin (Linder 2008) because they offer a means of measuring the growth rate of large-scale structures directly.

Currently, the most developed probes of cosmic acceleration originate from distance measurements but say very little about gravitational dynamics. However, a constraint on the growth rate may assist in breaking a possible degeneracy between models with the same expansion history but differing in terms of their gravitational physics. Few probes are as sensitive to gravitational dynamics as RSD; weak-lensing measures the integrated growth to some redshift, but not the growth rate. Pairwise velocity statistics of objects, e.g., supernovae, have been proposed to explore the growth rate, but this technique will not produce competitive constraints until a sufficiently high number density of objects are measured with a future survey such as the Large Synoptic Survey Telescope (Bhattacharya 2011).

The growth rate can be measured via RSDs to modest precision in recent and ongoing large galaxy redshift surveys, such as SDSS-II (Abazajian et al. 2009), VVDS (Le Févre et al. 2005), WiggleZ (Drinkwater et al. 2010), and BOSS (Eisenstein et al. 2011) that cover $z = 0.1$–0.9. In the next generation, surveys such as BigBOSS (Schlegel et al. 2009), SuMIRe (Suto 2010), and Euclid (Laureijs 2009) will provide precise measurements over an even greater range of redshifts up to $z = 2$.

In Section 2, we review the physics of RSDs from the galaxy velocity field. Section 3 discusses methods for accurately extracting the growth rate from the galaxy power spectrum. To compare analytic approximations from perturbation theory to the fully nonlinear solutions, we carry out *N*-body simulations in Section 4. In Sections 5–7, we investigate the bias induced in the growth rate due to the effects of nonlinearity in the density field as a function of the maximum wavenumber $k_{\rm max}$. These investigations are split into three classes of models: the Kaiser limit in Section 5, the quasi-linear Scoccimarro ansatz in Section 6, and the nonlinear models given by perturbation theory in Section 7. We perform a closer investigation of the appropriate form of the damping function and angular dependence in the redshift space power spectrum in Section 8, finding an accurate, scale-dependent correction factor, and in Section 9 we open the parameter space to discuss the implication of systematics on detecting deviations from general relativity. The conclusions of this paper are presented in Section 10.

2. GALAXY VELOCITY FIELDS

On large scales, the peculiar velocities of galaxies are dominated by the bulk flow motions induced by the gradients of gravitational potentials. These in turn arise from mass density fluctuations and so the velocity field traces the growth rate of large-scale structure. The continuity equation gives the relationship between the density and velocity fields and in the linear

density regime is written as

$$\nabla \cdot v(\mathbf{x}) = -f\,\delta(\mathbf{x}), \tag{1}$$

where δ, the density perturbation, is defined in terms of the density ρ and its mean value $\bar{\rho}$ such that $\delta = (\rho - \bar{\rho})/\bar{\rho} \ll 1$, D is the linear growth factor so $\delta(a) \propto D(a)$, and $f \equiv d\ln D/d\ln a$ is the linear growth rate.

The peculiar velocities add an extra component to the cosmological redshift which perturbs the real space positions of galaxies, x_r, along the line of sight:

$$x_s = x_r + (1+z)\frac{\mathbf{v}_{\rm pec}\cdot\hat{\mathbf{x}}}{H(z)}, \tag{2}$$

where x_s is the redshift space position and $\hat{x}$ is the direction of the line of sight. The expansion rate, or Hubble parameter, $H(a) = d\ln a/dt$ and the redshift $z = a^{-1} - 1$. This apparent change in position produces an additional anisotropic component to the power spectrum or correlation function because the amount of shifting that occurs is dependent on the angle made with respect to the line of sight.

The growth rate f can be extracted from measurements of the mass density power spectrum, in the combination $f(z)\,\sigma_8(z)$ (Percival & White 2009), where σ_8 is the rms mass fluctuation amplitude proportional to the growth factor $D(a)$. Thus, $f\sigma_8 \propto d\,D/d\ln a$. Within general relativity, the growth is determined by the expansion history $H(a)$ (assuming negligible dark energy clustering or interaction). To separate the effects of the expansion from any modifications to the standard gravity picture, Linder (2005) introduced the gravitational growth index γ, which parameterizes the true linear growth rate f as

$$f \approx \Omega_m(a)^{\gamma}\,, \tag{3}$$

for models that are matter dominated at high redshift and has been shown to be accurate to the subpercent level (even better for $f\sigma_8$) for a number of classes of cosmological models.

The gravitational growth index γ provides a useful extension to the cosmological model framework, allowing straightforward tests of growth versus expansion, and a compact method for distinguishing between many classes of modified gravity models. For instance, a ΛCDM model has $\gamma = 0.55$, with almost no dependence on the dark energy equation of state w, whereas for a Dvali Gabadadze Porrati gravity model (Dvali et al. 2000), $\gamma = 0.68$ and for many $f(R)$ gravity models, $\gamma \approx 0.42$ today. We will explore therefore not only the measurement of the growth rate f, but also its propagation into cosmological parameter estimation of the matter density Ω_m, the dark energy equation of state, and the gravitational growth index γ.

Current measurements of f have been made from galaxy redshift surveys from the Two-Degree Field (Hawkins et al. 2003) and the Sloan Digital Sky Survey (SDSS; Samushia et al. 2011 and older measurements) at low redshift; and at higher redshifts using VVDS (Guzzo et al. 2008) and WiggleZ (Blake et al. 2011). These have constrained $f\sigma_8$ at particular redshifts to $\sim$10% at best, but the precision and redshift coverage are not yet sufficient to stringently test for modifications to gravity. Nonetheless, they are exciting precursors to the constraints that will be produced by BOSS and BigBOSS. As the measurements get more precise, it is important to ensure that the analysis methods and theoretical knowledge keep pace in their accuracy.

Linder (2008) demonstrated that once f was extracted from next generation measurements of RSDs one could place significant constraints on γ and theories of gravity. Propagating errors, one sees that at a single redshift the relation between the uncertainties on f and γ is

$$\frac{\delta f}{f} = \gamma\,\frac{\delta\Omega_m(a)}{\Omega_m(a)} + \ln\Omega_m(a)\;\delta\gamma\,. \tag{4}$$

For an experiment to determine γ say to 0.04, we would require a 2% measurement of f at $z = 0.5$ or a 1% measurement at $z = 1$ if we knew the expansion history to precisely follow a ΛCDM concordance cosmology. Without perfect knowledge of $\Omega_m(a)$, the constraint on f would need to be tighter to achieve the same precision on γ. Thus the ability to measure accurately f from a survey is a crucial topic to investigate. This article investigates the impact of various systematics on the quality of cosmological constraints as we approach the precision required to produce strong tests of our understanding of gravity.

Methods for realistically extracting the growth rate from the measured galaxy power spectrum have been studied by, e.g., Okumura & Jing (2011) in the linear regime and Percival & White (2009) and Jennings et al. (2011a) in the quasi-linear regime. We extend their analyses by investigating more fully the effects of including nonlinearities and their impact on a broader set of cosmological parameters that are expected to influence measurements of the growth rate. We test how well various models for RSDs perform, focusing on three redshifts, $z = 0, 0.5, 1$ with three cuts in scale: $k_{\rm max} = 0.07\,h$ Mpc^{-1} to test RSD on large scales well in the linear regime, $k_{\rm max} = 0.1\,h$ Mpc^{-1} at the onset of nonlinearity, and $k_{\rm max} = 0.2\,h$ Mpc^{-1} to investigate the nonlinear regime, although it is really distinctions such as these that we are aiming to probe.

3. REDSHIFT SPACE DISTORTION THEORY

RSDs introduce an anisotropic component to the power spectrum, as the peculiar velocity of the galaxy projected along the line of sight adds to the cosmological redshift, perturbing the galaxy positions. This occurs as a bulk effect, and to be able to reliably extract the growth rate from it we need to measure a statistic such as the power spectrum of density fluctuations or the spatial correlation function, which quantify the degree to which objects cluster. In this work, we consider the power spectrum because of its close relationship with theory and the ease with which a linear power spectrum may be obtained from a Boltzmann code such as CAMB (Lewis et al. 2000). Other works have utilized the correlation function instead to investigate RSD, such as Guzzo et al. (2008) and Tocchini-Valentini et al. (2011).

The complete, nonlinear redshift space power spectrum is given by

$$P^s(\mathbf{k}) = \int \frac{d^3r}{(2\pi)^3} e^{-i\mathbf{k}\cdot\mathbf{r}} \langle e^{if k\mu\Delta u_z}[1+\delta(\mathbf{x})][1+\delta(\mathbf{x}')]\rangle, \tag{5}$$

as presented in Scoccimarro (2004), where $\mathbf{k}$ is the wavevector, $\mathbf{r} = \mathbf{x}' - \mathbf{x}$, $\Delta u_z = u(\mathbf{x}') - u(\mathbf{x})$ and u is the peculiar velocity field expressed in comoving coordinates such that $u = v_{\rm pec}/H$. Even though we can write down the full expression, it involves quantities, such as the nonlinear density contrast $\delta(\mathbf{x})$, that we cannot easily link to theoretical predictions when given a set of cosmological parameters, and thus the growth rate cannot be extracted this way.

In the linear density limit, the above equation reduces to something tractable known as the Kaiser formula (Kaiser 1987):

$$P^s(k,\mu) = (b + f\mu^2)^2 P_{\delta\delta}(k), \tag{6}$$

where μ is the cosine of the angle made by $\mathbf{k}$ with respect to the line of sight ($\mathbf{r}$ in Equation (5)), thus making an essentially two-dimensional power spectrum involving radial (line of sight) and transverse modes. This anisotropy is in contrast to the undistorted linear matter power spectrum $P_{\delta\delta}$. Note that b is the linear bias factor, relating the galaxy density fluctuations to the mass fluctuations. Equation (6) is a result of several assumptions imposed on the full relationship between real and redshift space in Equation (5), which we explore in Section 5.

To extend RSD theory to smaller scales, several quasi-linear and nonlinear models have been proposed. The full linear model for RSDs includes a velocity streaming term in the form of an extra exponential damping term,

$$P^s(k,\mu) = e^{-(fk\mu\sigma_v)^2}(b+f\mu^2)^2 P_{\delta\delta}, \quad (7)$$

where $\sigma_v^2 = [1/(6\pi^2)]\int P_L\, dk$ and P_L is the linear power spectrum (Fisher 1995). Within the Kaiser limit, this multiplication/convolution accounts for the joint density and velocity probability distributions along the line of sight in Fourier/real space assuming that the pairwise velocity probability distribution function (PDF) is Gaussian.

Fisher (1995) inspired others to take a similar approach to modeling the more nonlinear finger-of-God (FoG) effect (see Jackson 1972; Sargent & Turner 1977 for early discussions), and an additional small-scale velocity dispersion term $\sigma_{\rm vir}$ arises from convolving the pairwise velocity dispersion profile of objects within a halo with the linear Kaiser or streaming model. Assuming a Gaussian profile for random motion of galaxies within virialized structures results in the exponential damping term proposed by Peacock & Dodds (1994), while using an exponential profile for the velocity dispersion, first derived by Peebles (1976) and then applied to the power spectrum by Park et al. (1994), results in a Lorentzian damping term. Such a combination is often then taken to be the full quasi-linear model of RSDs (Desjacques & Sheth 2010),

$$P^s(k,\mu) = e^{-(fk\mu\sigma_v)^2} V_{\rm vir}(k,\mu)(b+f\mu^2)^2 P_{\delta\delta}\,, \quad (8)$$

where $V_{\rm vir} = \exp[-(k\sigma_{\rm vir}\mu)^2]$ for the Gaussian profile or $V_{\rm vir} = (1+k^2\sigma_{\rm vir}^2\mu^2)^{-1}$ for Lorentzian damping. These are of course the same to first order. Note that σ_v and $\sigma_{\rm vir}$ are not identical in general because σ_v quantifies the bulk motion of objects, for example halos, while $\sigma_{\rm vir}$ aims to model small-scale motion, such as that of bound objects within a halo.

However, Equations (7) and (8) are still linear in the sense that the densities and velocities are assumed to be exactly coherent such that the bulk flow of the dark matter traces out the velocity divergences exactly and $P_{\theta\theta} = f^2 P_{\delta\delta}$ and $P_{\delta\theta} = -fbP_{\delta\delta}$. The simplest of the models that accounts for the additional information contained in the nonlinear power spectrum of velocity divergences is the ansatz proposed in Scoccimarro (2004),

$$P^s(k,\mu) = e^{-(fk\mu\sigma_v)^2}[b^2 P_{\delta\delta}(k) - 2\mu^2 P_{\delta\theta} + \mu^4 P_{\theta\theta}], \quad (9)$$

where $P_{\delta\delta}$, $P_{\delta\theta}$, and $P_{\theta\theta}$ are the *nonlinear* density, density-velocity, and velocity divergence power spectra, defined as $P_{\delta\theta} = \langle|\,\delta\theta^*|\rangle$ and $P_{\theta\theta} = \langle|\theta|^2\rangle$, where $\theta = \nabla\cdot\mathbf{v}$. The velocity dispersion is given by σ_v^2 as defined in Equation 7. Jennings et al. (2011b) demonstrated that this recovers the linear growth rate up to $k = 0.25\,h$ Mpc^{-1} to a precision on f of 0.64%, but it is difficult to predict $P_{\delta\delta}$, $P_{\delta\theta}$, and $P_{\theta\theta}$ in the fully nonlinear regime without recourse to N-body simulations.

One of the most promising avenues for treating RSDs is to take a perturbative approach to the full transformation (Equation (5)) and expand the term within angular brackets. The most widely used and simplest perturbative scheme is standard perturbation theory (SPT), in which the expansion is performed in powers of the scale factor (see Jain & Bertschinger 1994 for more details). Such schemes are expected to model the nonlinear effects to higher accuracy than Equation (9), since that model does not constitute an exact expression under perturbation theory as previously noted by Matsubara (2008) and Taruya et al. (2010). Some caution is required; no single perturbative scheme is preferred, they each have their regimes of validity (Carlson et al. 2009), and they are limited to being useful only when the situation is mostly linear but requires a small correction. The demarcation between linear and nonlinear regimes is often different in redshift and real space and some perturbation theories have a more limited range of accuracy in redshift space (Scoccimarro et al. 1999). Some of these problems are addressed by using other perturbative schemes such as renormalized perturbation theory (RPT) and closure theory.

Perturbation theory adds additional terms to the Kaiser formula to model the nonlinear contributions to the redshift space power spectrum. The next to linear order in the SPT expansion of the real space power spectrum is the 1-loop expression given by

$$P(k) = P_L + P_{13} + P_{22}, \quad (10)$$

where P_L is the linear power spectrum and P_{13}, P_{22} are mode coupling terms containing extra corrections to third order in δ_k. For redshift space, these terms are

$$P^s(k,\mu) = (b+f\mu^2)^2 P_L + (b+f\mu^2)P_{13}^s + P_{22}^s \quad (11)$$

as derived by Heavens et al. (1998), Scoccimarro et al. (1999), and Matsubara (2008), and we refer the reader to these works for the complete expression. Both mode coupling terms in Equation (11) now contain additional redshift space contributions that are sensitive to the growth rate. In Lagrangian perturbation theory (LPT), this becomes

$$P^s(k,\mu) = e^{-k^2(1+f(f+2)\mu^2)\sigma_v^2}\big[(b+f\mu^2)^2 P_L + (b+f\mu^2)P_{13}^s + P_{22}^s + (b+f\mu^2)^2 P_L k^2(1+f(f+2)\mu^2)\sigma_v^2\big], \quad (12)$$

as derived by Matsubara (2008). An exponential damping term naturally arises in the derivation that accounts for both BAO damping and RSD smearing. Although some of the mode coupling terms look formidable, these equations are not too difficult to derive and evaluate. However, the expressions beyond the 1-loop terms are much more computationally demanding; the presence of mode coupling produces multidimensional integrals that need to be performed numerically and that can be as time consuming as running an entire N-body simulation. This is far too expensive to be done in the course of a parameter fitting routine during which the model power spectrum may need to be evaluated at each point in parameter space.

Another popular perturbation scheme is closure theory, in which higher order N-point statistics, such as the bispectrum, are defined in terms of derivatives of lower order N-point statistics to close the system of equations. The closure theory expansion of the redshift space power spectrum derived by Taruya et al.

(2010, hereafter known as Taruya^{++}), produces additional terms in the Scoccimarro formula, and Equation (9) is now

$$P^s(k,\mu) = e^{-(fk\mu\sigma_v)^2}[b^2 P_{\delta\delta}(k) - 2\mu^2 P_{\delta\theta} + \mu^4 P_{\theta\theta} + b^3 A(k,\mu,f,b) + b^4 B(k,\mu,f,b)], \quad (13)$$

where $A(k,\mu,f,b)$ and $B(k,\mu,f,b)$ contain the extra contributions to the power spectrum arising from the coupling of the density and velocity fields (see Taruya et al. 2010 for the full terms), which are rather lengthy to calculate even in an era where computational power is cheap. These three models, SPT, LPT, and closure theory, comprise the main perturbative approaches to modeling the RSD power spectrum.

4. *N*-BODY SIMULATIONS

Finding a robust approach to extracting growth rate information requires comparison to the nonlinear power spectra as given by simulations. The simulations were performed using GADGET2 (Springel 2005) with a box of length 1500 Mpc h^{-1} per side and 1024^3 particles and a particle mass of $\approx 2.2 \times 10^{11} M_\odot\ h^{-1}$. We chose a reference ΛCDM cosmology with $\Omega_{m,0} = 0.25$, $\Omega_{\Lambda,0} = 0.75$, $\Omega_{b,0} = 0.045$, $n_s = 0.97$, $\sigma_8 = 0.8$, and $h = 0.72$.

There are numerous factors that affect the ability of an *N*-body simulation to accurately reproduce the growth of structure but we will only outline the most significant effects that could impact our results. The box size was chosen to be large enough so that the growth of the modes on the scales of interest could be fed with a sufficient number of larger modes via mode coupling. The initial conditions for the simulations were obtained using the Zel'dovich approximation (Zel'dovich 1970) evaluated at $z = 199$; this is a sufficiently high redshift to prevent an artificial damping of the power spectrum that occurs when the modes are not given enough time for nonlinear growth (Heitmann et al. 2010). We ran 20 simulations with the same cosmological parameters but each simulation is initialized by a different realization of a Gaussian field set by the fiducial cosmology. We also ran a number of simulations with different box sizes, particle numbers, and error tolerances in the gravity calculations to ensure numerical convergence. Each simulation contributes three projections of a redshift distorted density field from the three lines of sight oriented along each axis of the box, which we average over as in Guzzo et al. (2008), Percival & White (2009), and Jennings et al. (2011a). Although the density modes of each projection shared the same growth history, the distribution of particles seen along each axis is now different and each redshift space power spectrum contains new information. This gives a final space power spectrum that has been averaged over 20 realizations with each simulation contributing three projections of the redshift space power spectrum. As an accuracy test of our simulations, we have compared our real space power spectrum averaged over all the realizations to the power spectrum emulator in Lawrence et al. (2010) and found a dispersion of less than 2% between the power spectra (1% with Halofit (Smith et al. 2003)) over the scales we consider in this article. The real space density and redshift space power spectra are measured by applying the method outlined in Jing (2005) with a third-order mass assignment scheme (triangular shaped cloud (TSC)) to smooth the particles on to a fast Fourier transform (FFT) grid size of 2048^3 for the density power spectra. The density-velocity and velocity power spectra, $P_{\theta\delta}$ and $P_{\theta\theta}$, also use a TSC mass assignment scheme but with an additional step that involves dividing by the densities to remove the mass weighting imposed by binning the particles (Scoccimarro 2004). Because of the sparseness of the particle density in certain regions of the simulation, we could only achieve a maximum FFT grid resolution of 512^3 for these power spectra.

The cosmological parameters were derived using the Metropolis algorithm of CosmoMC (Lewis & Bridle 2002) to facilitate a Markov Chain Monte Carlo (MCMC) process to calculate the likelihood distribution of these parameters assuming a particular model of RSD is true. The errors on the redshift space power spectrum were estimated using ∼1200 Gaussian realizations (depending on how many were required for the covariance matrix to converge) using the same volume but only 256^3 particles for speed. Applying the Zel'dovich approximation on the Gaussian density field then gives the velocities as

$$v(x) = aHfD\phi(x), \quad (14)$$

where ϕ is the potential for a particle located at x. For the smallest range in k, we were able to obtain the covariance matrix directly from the simulations and this provided a useful check against the errors given by the Zel'dovich approximation. We found that the resultant best-fitting values for the growth rate were almost indistinguishable for $0.03 < k < 0.07\,h$ Mpc^{-1}. A linear theory power spectrum P_L is produced by CAMB using the parameterized post-Friedmann module (Fang et al. 2008) to treat the perturbations in the fluid equations for $\{w_0, w_a\}$ models, where the dark energy equation of state is given by $w(a) = w_0 + w_a(1-a)$. Utilizing the linear theory power spectrum, we have implemented SPT, LPT, and Taruya^{++} theory schemes for the real and redshift space power spectra within CosmoMC in order to explore the full parameter range that affects growth. The growth rate is modeled either in terms of f or γ as an additional free parameter. We consider a chain to have converged when $R - 1 \leqslant 0.01$, where R is defined as the ratio of the variance between the mean of the chains and mean of the chain variance.

5. LIMITS OF THE KAISER FORMULA

The Kaiser formula has already been demonstrated to have a limited range of applicability by Jennings et al. (2011a, 2011b) and Okumura & Jing (2011) and most notably by Scoccimarro (2004) but despite these shortcomings has been applied to a number of data sets, most of these at low redshift, deep in the nonlinear regime. Okumura & Jing (2011) and Jennings et al. (2011b) showed that the Kaiser formula is unable to reproduce the growth rate measured from an *N*-body simulation on all but the very largest scales, especially for low-mass halos. We revisit the problem using the original Kaiser formula as presented in Kaiser (1987) but then extend our analysis to address its various extensions such as the streaming model (Fisher 1995) and the various quasi-linear FoG damping models that have been proposed (Peacock & Dodds 1994; Park et al. 1994). The analysis of the Kaiser limit in this section provides a point of comparison for the results of the higher order models that we analyze in Sections 6 and 7.

Figure 1 shows the marginalized 1σ confidence limits on the growth rate obtained from fits to the full redshift space dark matter power spectrum in $\{k,\mu\}$ with 20 bins in μ measured from an ensemble of *N*-body simulations at $z = 0, 0.5, 1$. The only parameters that are allowed to vary are the growth rate f and the linear bias, b, while all others are kept fixed at their fiducial value, with the exception of the empirical damping model which has σ_v as an additional free parameter. We have checked that the

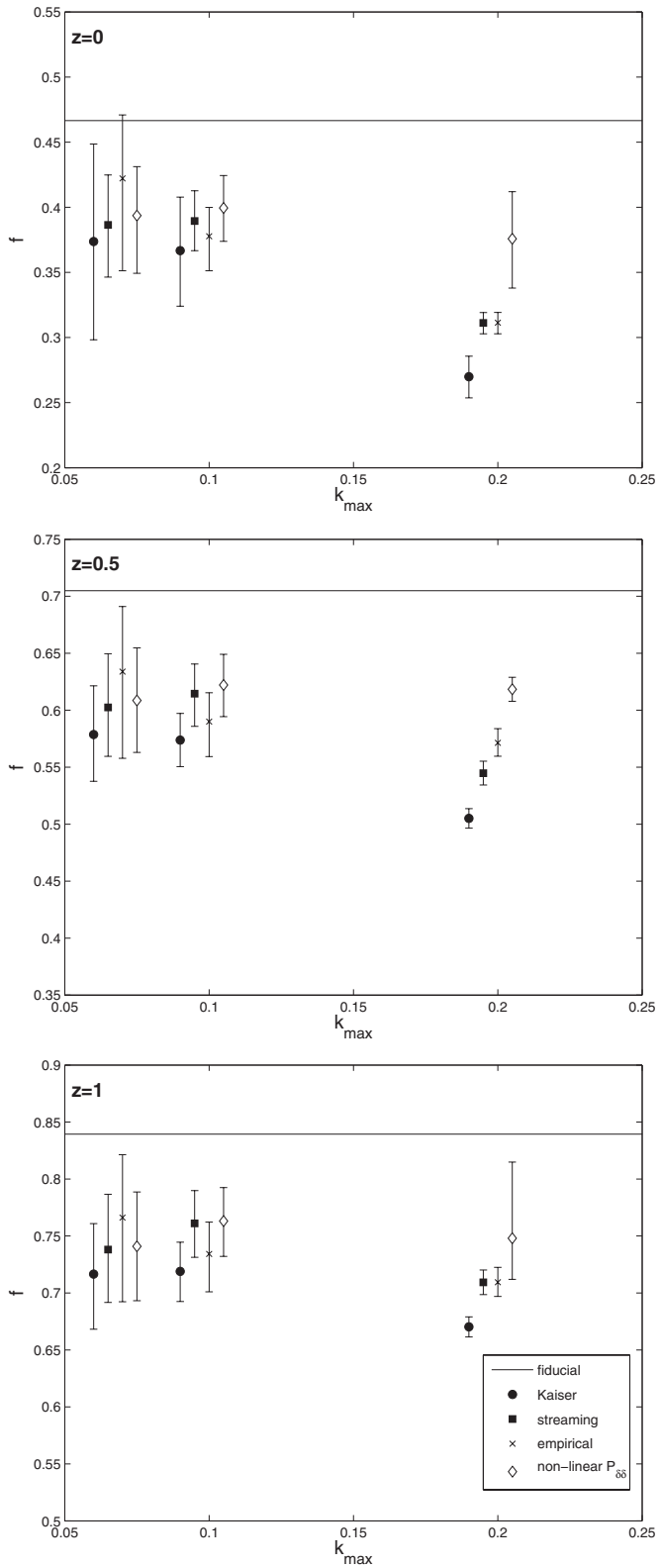

Figure 1. Constraints on the growth rate using the various Kaiser-type models of the redshift space power spectrum evaluated at $z = 0$ (top), $z = 0.5$ (middle), and $z = 1$ (bottom), with cutoffs at $k_{\rm max} = 0.07, 0.1, 0.2\,h$ Mpc^{-1}. All the models are biased; the horizontal lines show the true value of f at each redshift. The fitted parameters are $\{f, b\}$, and σ_v in the case of empirical damping. Note that some points have been offset by a small amount in $k_{\rm max}$ for clarity.

best-fitting value of the growth rate remains the same within 1σ when the linear bias is fixed to $b = 1$ up to $k_{\rm max} = 0.1\,h$ Mpc^{-1}. However, at $k_{\rm max} = 0.2\,h$ Mpc^{-1}, we found that the behavior was model dependent; sometimes this moved the fit closer to the fiducial growth rate but in all circumstances, the 1σ region did not lie within the true value anyway.

We have quoted the mean likelihoods obtained from CosmoMC, rather than the best fitting points, because these are considered to be more robust against variations in chain length (Lewis & Bridle 2002), although the differences are minor. The 1σ intervals are calculated from the one-dimensional minimum credible intervals obtained from the posterior by using two tailed equal likelihood limits. We consider four different models for the redshift space power spectrum: the Kaiser limit (Equation (6)), the streaming model (Equation (7)), the streaming model with nonlinear $P_{\delta\delta}$, and the empirical model which has the same form of exponential damping as the streaming model, but σ_v is treated as a free parameter. These models and their free parameters are listed in the top third of Table 1.

Each of the four models was fitted to a redshift space power spectrum measured from N-body simulations with three cuts in k, namely, $k_{\rm max} = 0.07, 0.1, 0.2\,h$ Mpc^{-1}. For each of these power spectra, $k_{\rm min} = 0.03\,h$ Mpc^{-1}, since the larger modes have been contaminated by the finite box size. This large-scale cutoff was determined by comparing the real space power spectrum measured from the simulations to a reference power spectrum supplied by the CosmicEmu package (Lawrence et al. 2010). We have also performed additional convergence tests in redshift space at an extremely high redshift of $z = 19$ to confirm that on these scales we could recover the Kaiser limit (Equation (6)) with our N-body redshift space power spectrum.

The performances of these Kaiser-type models are unimpressive regardless of scale and redshift, even for $k_{\rm max} = 0.07\,h$ Mpc^{-1} at $z = 1$ where it is commonly thought that structure formation might be sufficiently linear that the Kaiser model might be appropriate. While the failure of the Kaiser limit is broadly consistent with the findings of Okumura & Jing (2011) and Jennings et al. (2011b), in that the growth rate is underpredicted by these models, it is a little surprising that neither the damping term nor the inclusion of the nonlinear power spectrum affects the best-fitting value for the growth rate. All these variants of the Kaiser limit assume that $P_{\theta\theta} = f^2 P_{\delta\delta}$ and $P_{\delta\theta} = -bf P_{\delta\delta}$, and the bias in these models regardless of damping suggests that neglecting to include the nonlinearity of large-scale motions by their simplistic relationship between density and velocity, rather than the smearing of power from FoG effects, is the most important systematic at low redshifts (Scoccimarro 2004; Jennings et al. 2011a). But it is not until we examine the Scoccimarro and Taruya^{++} models in Sections 6 and 7 that we can see the significance of the coupling between the density and velocity fields; the extra terms in the Taruya^{++} formalism affects scales as large as $k_{\rm max} = 0.07\,h$ Mpc^{-1}.

Even though the streaming model accounts for the coupling between the density and velocity fields with the factor of $\exp(-f^2k^2\mu^2\sigma_v^2)$, the assumption that the velocity distribution is Gaussian with a scale-independent dispersion term was shown to be of limited applicability by direct comparison to N-body simulations in Scoccimarro (2004). Neither does exchanging the linear for the nonlinear matter power spectrum in the Kaiser formula work; this merely shifts the power spectrum in k, μ downward to smaller k, while leaving the μ dependence the same. In fact, it is the functional dependence on μ in these RSD models that is inadequate, as suggested by the bias in the empirical model, which is allowed to adjust for as much exponential damping as required by the simulations. This

Table 1
List of Models Considered, Their Free Parameters, and Mentions in Other Literature

Model	Parameters	Equation		References
Kaiser	f, b	$P^s(k,\mu) = (b + f\mu^2)^2 P_L(k)$	[6]	Kaiser (1987)
Streaming	f, b	$P^s(k,\mu) = e^{-(fk\mu\sigma_v)^2}(b + f\mu^2)^2 P_L(k)$	[7]	Fisher (1995)
Empirical	f, b, σ_v	As above but σ_v is a free parameter	[7]	Samushia et al. (2011)
Nonlinear $P_{\delta\delta}$	f, b	As for streaming but P_L is replaced by nonlinear $P_{\delta\delta}$	[7]	Blake et al. (2011)
Scoccimarro (with linear damping)	f, b	$P^s_q(k,\mu) = e^{-(fk\mu\sigma_v)^2}[b^2 P_{\delta\delta}(k) - 2\mu^2 P_{\delta\theta} + \mu^4 P_{\theta\theta}]$	[9]	Scoccimarro (2004)
Scoccimarro (with empirical damping)	f, b, σ_v	As above but σ_v is a free parameter	[9]	Scoccimarro (2004) Jennings et al. (2011b)
SPT	f, b	$P^s_{\rm SPT}(k,\mu) = (b + f\mu^2)^2 P_L + (b + f\mu^2) P^s_{13} + P^s_{22}$	[11]	Heavens et al. (1998) Scoccimarro et al. (1999) Matsubara (2008)
LPT	f, b	$P^s_{\rm LPT} = e^{-k^2(1+f(f+2)\mu^2)\sigma_v^2} \times [P^s_{\rm SPT} + (b + f\mu^2)^2 P_L k^2 (1 + f(f+2)\mu^2)\sigma_v^2]$	[12]	Matsubara (2008)
Taruya^{++} (with linear damping)	f, b	$P^s(k,\mu) = P^s_q + e^{-(fk\mu\sigma_v)^2} \times [b^3 A(k,\mu,f,b) + b^4 B(k,\mu,f,b)]$	[13]	Taruya et al. (2010)
Taruya^{++} (with empirical damping)	f, b, σ_v	As above but σ_v is a free parameter	[13]	Taruya et al. (2010)

Notes. We have divided this table into three sections, corresponding to Sections 5–7 as we progress down the table. Note that empirical damping means that we allow the MCMC process to decide the amount of damping necessary for a good fit.

angular dependence is a key point, and we explore it further in Section 8.

Figure 2 shows the full two-dimensional redshift space power spectra of the models of this section (for simplicity we do not show the empirical model) compared to the N-body power spectrum. We have shown these as a function of k and μ, instead of in the $k_\perp$–$k_\parallel$ plane, because we find it useful to fit in terms of k and μ so these figures provide a direct point of comparison. None of these models are predicting the correct behavior at small angles (i.e., large μ) and even on large scales (i.e., small k). Looking at Figure 2, we can see that the streaming and empirical damping models work in an average sense via a happy coincidence: the linear theory matter power spectrum underpredicts the amount of damping required at large μ, but happens to compensate for this by predicting less power at $\mu \sim 0$, i.e., the real space power spectrum is smaller than it ought to be.

The inability of the Kaiser-type formulae to predict an adequate amount of damping in the power spectrum as μ approaches unity suggests that it may be worthwhile to consider truncating the power spectrum in $k\mu$ instead of just scale alone. Unfortunately, we found that for even quite conservative cuts such as $k\mu < 0.05\,h$ Mpc^{-1} and $k < 0.2\,h$ Mpc^{-1}, no substantial improvements could be gained: the growth rate is still biased by more than 1σ despite the increase in the error bars because of the weaker dependence on f. Nonetheless, we would like to investigate the limit at which k and $k\mu$ can be truncated to reproduce the streaming model with reasonable constraints on f, which doubles as a consistency test. We found that the scales considered were prohibitively large (no smaller than $k_{\rm max} = 0.07\,h$ Mpc^{-1} could be allowed) but the best-fitting values of f obtained were within 1σ of the fiducial. In Figure 2, the hyperbolic red curves show a contour of $k\mu$, and we find in Section 8 that an accurate fitting function in terms of $k\mu$ can allow us to extend robust extraction of the growth rate f to higher k. Furthermore, in Section 8 we show that to truly account for FoG nonlinear effects, we must allow for a damping term—or rather an amplification term—on small scales acting perpendicularly to the line of sight.

6. QUASI-LINEAR MODELS

As a next step, we investigate the Scoccimarro ansatz which presents a simple extension to the Kaiser formula beyond linear theory using the same techniques presented in Section 5. We use Equation (9) to model the redshift space power spectrum and extract the growth rate. To calculate $P_{\delta\delta}$, $P_{\delta\theta}$, and $P_{\theta\theta}$, we use 1-loop SPT which was shown to be accurate in $P_{\delta\delta}$ to 1% upto $k = 0.08\,h$ Mpc^{-1} at $z = 0$ in real space by Carlson et al. (2009) and a few percent for $P_{\delta\theta}$ and $P_{\delta\delta}$ to $k = 0.1\,h$ Mpc^{-1} at the same redshift (see Figure 8 of Carlson et al. 2009 for a detailed comparison. Note that the accuracy is comparable with improved PT).

There is a minor improvement from the Kaiser formula to the Scoccimarro results shown in Figure 3, which is not sufficient to produce an unbiased result to 1σ. Even on large scales, such as for $k_{\rm max} < 0.07\,h$ Mpc^{-1}, there is still a small difference between the Kaiser limit and the Scoccimarro ansatz, and both mean likelihoods are still skewed below the fiducial. This is rather unlikely to be the effect of the size of the simulation because the effect is model dependent, and changing the RSD model helps to improve the fit as we shall see in Section 7.

Curiously, the Scoccimarro points in black seem to improve as the cut in $k_{\rm max}$ loosens, particularly at $z = 0$ where the smaller scales are weighted more strongly. The growth rate is being overestimated as $k_{\rm max}$ increases because the large scales underestimate f while the small scales tend to overestimate it. We can see this effect at work in Figure 3, in which we have also explicitly split the k range into two intervals, showing the high range in red (the low range is given by the usual $k_{\rm max} = 0.1\,h$ Mpc^{-1} point). If the range of our fits to larger scales has an upper limit in the range $0.1 < k_{\rm max} < 0.2\,h$ Mpc^{-1}, then we could coincidentally obtain a growth rate that is consistent with the fiducial value. The interpretation is slightly more complicated with the Scoccimarro model than in the Kaiser limit because there are two competing effects; the real space power spectrum, $P_{\delta\delta}$, is underestimated by SPT on small scales but the real space $P_{\delta\theta}$ and $P_{\theta\theta}$ power spectra in SPT diverge in comparison to the N-body result. The former requires a growth

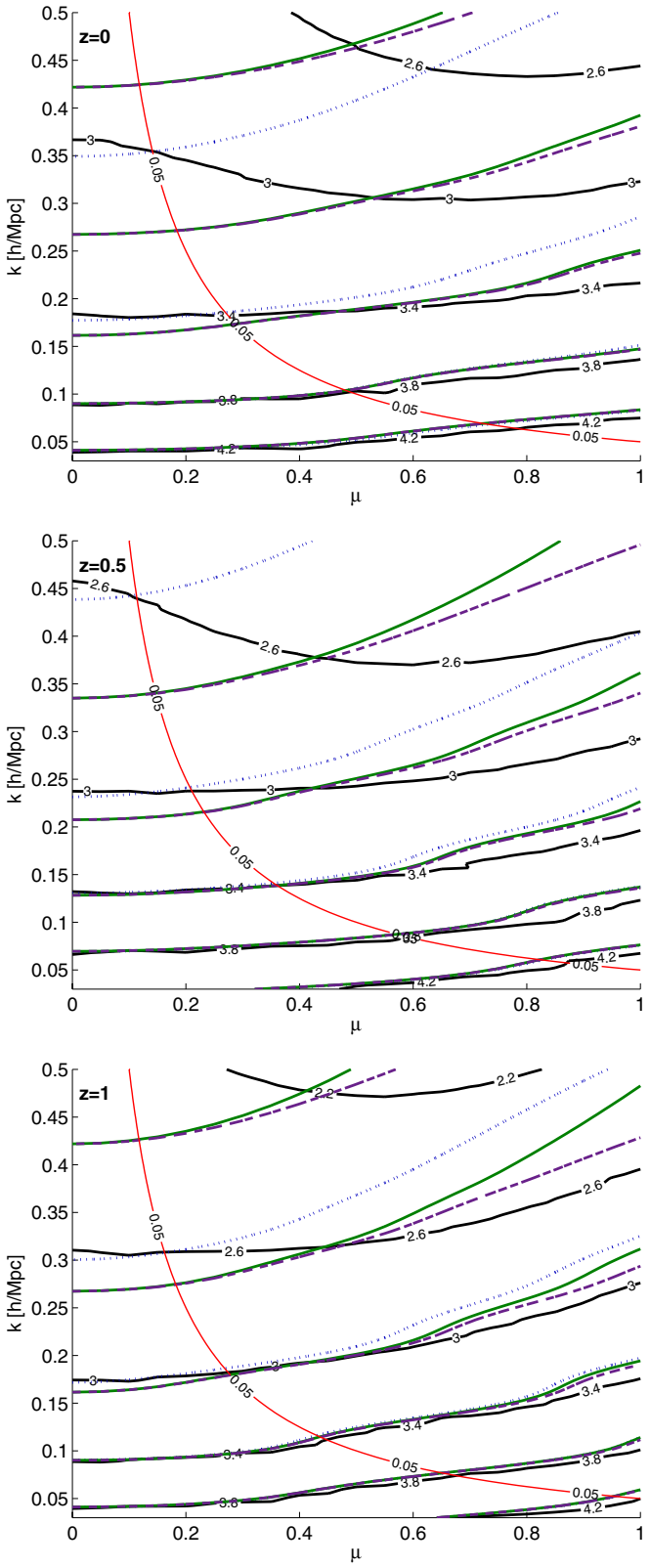

Figure 2. $P^s(k, \mu)$ for $z = 0, 0.5, 1$ calculated using the Kaiser limit without damping (dashed purple), the streaming model (solid green), and the streaming model using the nonlinear matter power spectrum (dotted blue), compared to measured redshift space power spectra from N-body simulations (black). The numbers on the black curves indicate the contour levels in $\log P^s(k, \mu)$. The hyperbolic red contours show constant $k\mu = 0.05\,h$ Mpc^{-1}. FoG effects are manifested in the amplification of the black contours at large k perpendicular to the line of sight ($\mu \approx 0$).

(A color version of this figure is available in the online journal.)

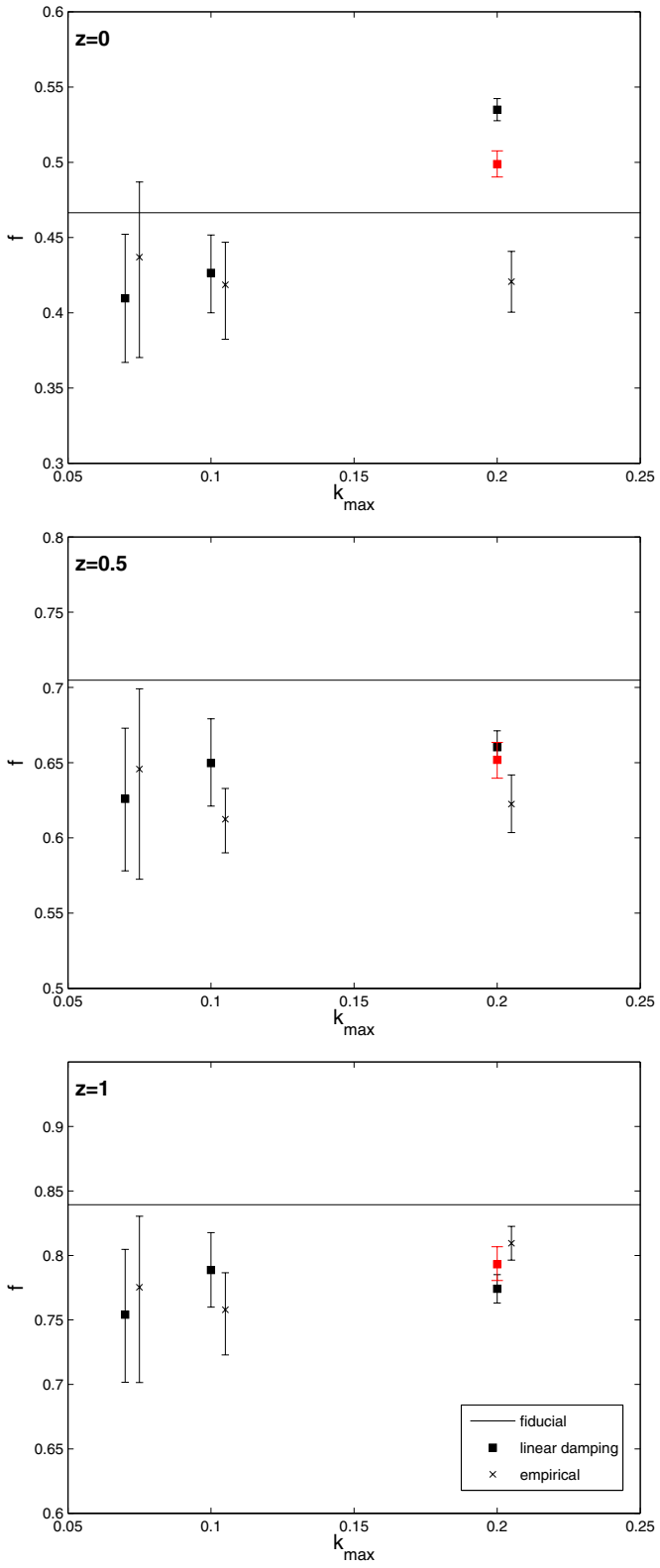

Figure 3. Same as Figure 1 but using the Scoccimarro ansatz with the real space nonlinear power spectra evaluated using SPT. We consider two types of damping in these fits, exponential damping with σ_v predicted by linear theory and allowing σ_v to be a free, empirical parameter. The light red squares at $k_{\rm max} = 0.2\,h$ Mpc^{-1} are the result of fitting only over the range $0.1 \leqslant k < 0.2\,h$ Mpc^{-1}.

(A color version of this figure is available in the online journal.)

rate to be larger than the fiducial value for the model to remain a good fit, while the latter favors a smaller value for the growth rate. The inconsistencies in the Scoccimarro ansatz are thrown into greater relief when we consider what the red points are telling us: fitting over the small and large scales jointly is not the same as fitting the small and large scales independently. A more familiar setting for this effect is the combination of two data sets, perhaps from different cosmological probes, that are inconsistent—their combined posterior distribution need not overlap a similar region in parameter space as their individual posteriors.

In addition, the use of empirical damping is unnecessary; in terms of 1σ confidence levels, the two models are indistinguishable at $k_{\rm max} < 0.1\,h$ Mpc^{-1} and both models are equally poor on smaller scales. Neither of these two models are able to consistently predict the correct value of the growth rate and both give a value that is substantially below the fiducial. This occurs because the model power spectrum does not predict enough damping on large scales particularly where the line-of-sight contribution is greatest; that is the nonlinear redshift space power spectrum has a lower amplitude than expected as $\mu \to 1$, but on small scales it is the reverse: FoG effects produce too much power perpendicular to the line of sight. This is explored in greater detail in Section 8.

Compared to the simulations of Jennings et al. (2011b), we find two areas of departure. Although our simulations have the same box size as theirs, the effective volume of our simulations obtained by averaging the power spectra over the full ensemble of realizations is substantially larger. For the complete set of simulations, we found weaker constraints on f and more biased fits for the Scoccimarro model. However, by only using half of the simulations, the scatter has increased such that we could obtain results that are consistent with the fiducial cosmology for the Scoccimarro model. Perhaps a more significant difference from Jennings et al. (2011b) is that we have used SPT for the real space power spectra instead of the fitting function of Jennings et al. (2011a). Although this offers a convenient alternative to perturbation theory, its accuracy is limited to scales larger than $k \approx 0.1\,h$ Mpc^{-1} because of the method used to measure $P_{\theta\theta}$. We elaborate on this fitting function in future work.

If we switch to using the exact forms for $P_{\delta\delta}$, $P_{\delta\theta}$, and $P_{\theta\theta}$ as measured from the suite of N-body simulations, we can separate the effects of the two approximations that are involved, since we are no longer dependent on the accuracy of SPT for the nonlinear power spectra. This model is represented in Figure 4 by the green contours, showing the redshift space power spectrum calculated with the Scoccimarro formula using linear theory damping but $P_{\delta\delta}$, $P_{\delta\theta}$, and $P_{\theta\theta}$ are measured directly from the N-body simulations. This is what would be produced by SPT if it were perfectly accurate up to $k \approx 0.2\,h$ Mpc^{-1}, but we caution that there will be a deviation from the true behavior of $P^s(k, \mu)$ on smaller scales because the resolution of the FFT grid is limited by the sparseness of the particles when calculating $P_{\theta\theta}$. Without the simulation results being available for every model, the results of the Scoccimarro ansatz could be improved over SPT by using a better approximation to calculate the real space power spectra such as RPT or a fitting formula such as Jennings et al. (2011a). One might be tempted to attribute the inadequacies of the Scoccimarro formula to the SPT power spectra, but this is surely not the case at large scales where SPT is valid to 1%. An inspection of Figure 4 shows that on these scales, there is a distinct difference between the Scoccimarro ansatz with linear theory damping and the N-body power spectrum even at $z = 1$. The unsatisfactory results obtained in this approach with SPT lead us to explore further perturbative schemes in the next section.

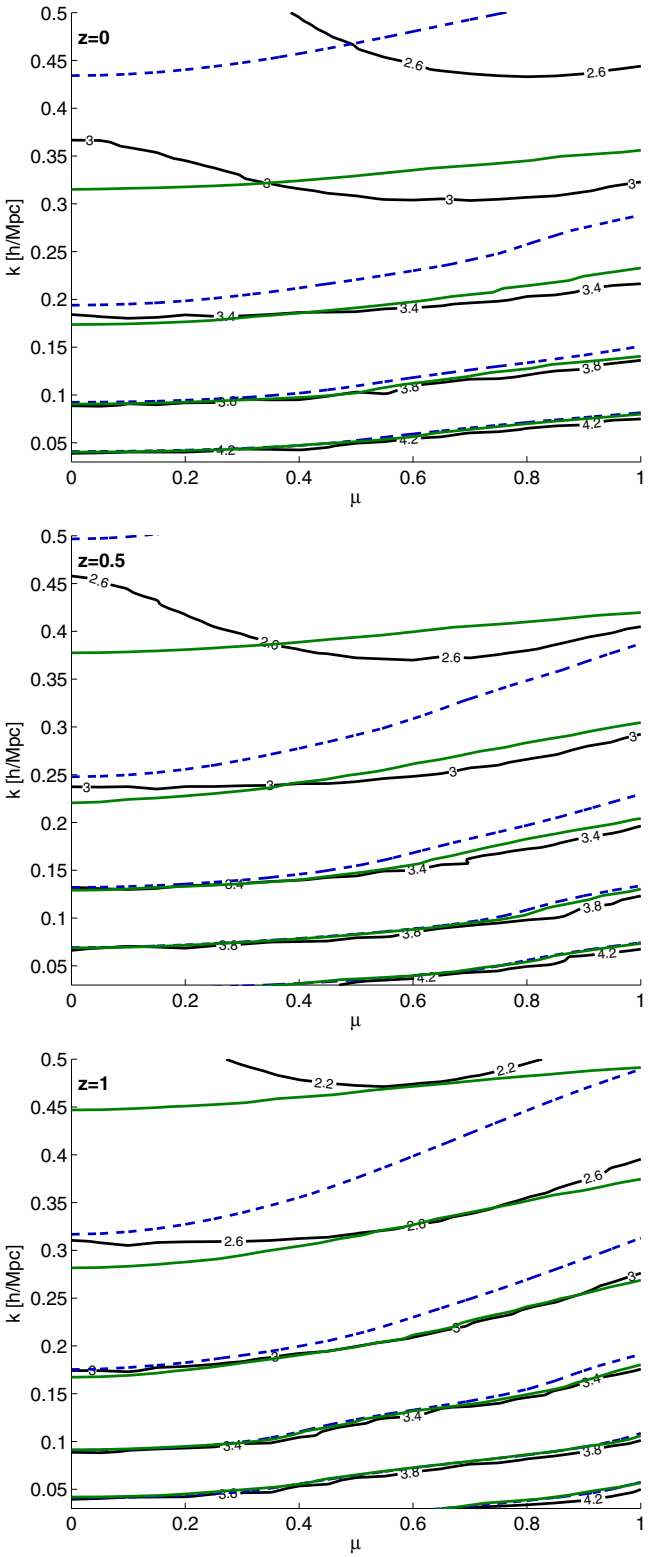

Figure 4. $P^s(k, \mu)$ for $z = 0, 0.5, 1$ as in Figure 2 but calculated using the Scoccimarro formula with linear theory damping, and $P_{\theta\theta}$, $P_{\theta\delta}$, and $P_{\delta\delta}$ measured from simulations (green) or 1-loop SPT (dashed blue), compared to the redshift space power spectrum from N-body simulations (black, labeled contours).

(A color version of this figure is available in the online journal.)

7. LIMITS OF PERTURBATION THEORY

We now consider more sophisticated models of RSDs, which are contained in the lower third of Table 1. These are the SPT models proposed by Heavens et al. (1998) and Scoccimarro et al. (1999) (Equation (11)), the LPT model of Matsubara (2008; Equation (12)), and model of Taruya et al. (2010; Equation (13)), which we refer to as Taruya^{++}. These models rely on first performing an expansion on the transformation from real to redshift space, and then the density contrast is given by an additional perturbative scheme in real space. To evaluate the terms in Equation (13), we have used SPT to obtain $P_{\delta\delta}$, $P_{\delta\theta}$, and $P_{\theta\theta}$ for ease of comparison with the previous Scoccimarro fits. Unlike the previous models that we have discussed, these models contain higher order terms beyond μ^4 up to μ^8. The values of f obtained from using these perturbation theory approaches are shown in Figure 5. Note that we calculate both the corrections suggested by the Taruya^{++} model and the $P_{\delta\delta}$, $P_{\delta\theta}$, and $P_{\theta\theta}$ used in Figure 5 using SPT.

Comparing Figures 3 and 5 (and the shapes of the power spectra in Figures 4 and 6), it is clear that both LPT and SPT models of RSD perform substantially *worse* than both the Kaiser and the Scoccimarro models. In fact, at $z = 0$ and $z = 0.5$ for $k_{\rm max} > 0.1\,h$ Mpc^{-1}, we were unable to obtain any constraints on f using these models, as the 1σ interval was consistent with 0. Within 1σ, the values of f given by LPT and SPT are indistinguishable, but the shape of the LPT power spectrum in Figure 6 is somewhat more reasonable, despite the damping term in LPT having a stronger dependency with μ. The bias of the growth rate is partially due to the strength of the constraints; the extra information contained in the higher order terms means that the errors on the growth rate are smaller. One of the advantages of considering terms beyond linear theory is the additional information contained in those extra terms that can break the degeneracy between f, b, and σ_8. For instance, although the fits are more biased in SPT and LPT, P^s_{22} and P^s_{13} contain different combinations of f, b, and σ_8 and some of these terms are proportional to $(f\sigma_8)^2\sigma_8^2$ and $(b\sigma_8)^2\sigma_8^2$.

But by far the dominant source of the discrepancy is that there are two levels of approximations that enter into the formalism: the density perturbation expansion and the mapping from real to redshift space. For the SPT redshift space power spectrum, the transformation from real to redshift space is expanded to third order and then the real space overdensities are perturbed to δ^3 for the 1-loop terms (Heavens et al. 1998). The derivation of the LPT redshift space power spectrum proceeds in a rather different manner, but the final expression can be related to SPT by expanding the linear theory damping term that is predicted self consistently in the theory (Matsubara 2008). The overall effect is to reduce the accuracy of perturbation theory in redshift space relative to its efficacy in real space. There are also several coincidental occurrences that are advantageous to the Kaiser and Scoccimarro formulae that are absent in the LPT and SPT redshift space power spectra.

The SPT and LPT models in fact miss important cross terms between the velocity and density fields that are included in the Taruya^{++} expression, see Equation (26) of Taruya et al. (2010). For this reason, the Taruya^{++} power spectrum is able to model the redshift space power spectrum with a smaller bias in the growth rate, as seen in Figure 5 on all scales and at all redshifts, but we found that the posteriors on b were biased beneath $b = 1$. It is worth noting, however, that all the redshift space power spectra considered in this section can be related to one another through the addition of extra terms in the perturbation theory expansion.

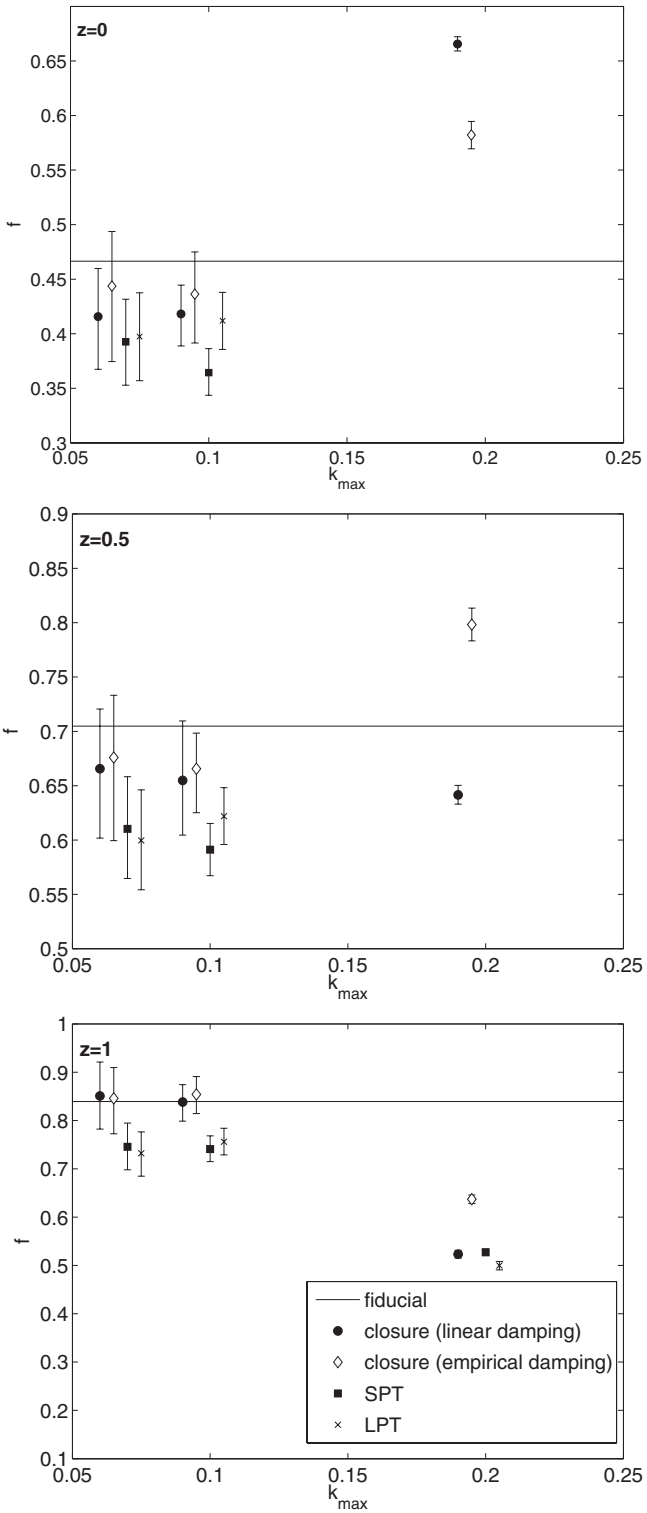

Figure 5. 1σ constraints on the growth rates derived from modeling the redshift space power spectrum with SPT, LPT, and Taruya^{++} (with linear theory and empirical damping) models of the full redshift space power spectrum. We have considered the Taruya^{++} model with both linear theory and empirical damping terms but the SPT model does not contain any damping. Values of f obtained for SPT and LPT have not been shown at $z = 0, 0.5$ for $k_{\rm max} = 0.2$ because they were consistent with zero.

Much of the variation in the estimates of the redshift space power spectrum obtained from perturbation theory originates from a judicious choice of terms to sum in the expansion of the density contrast.

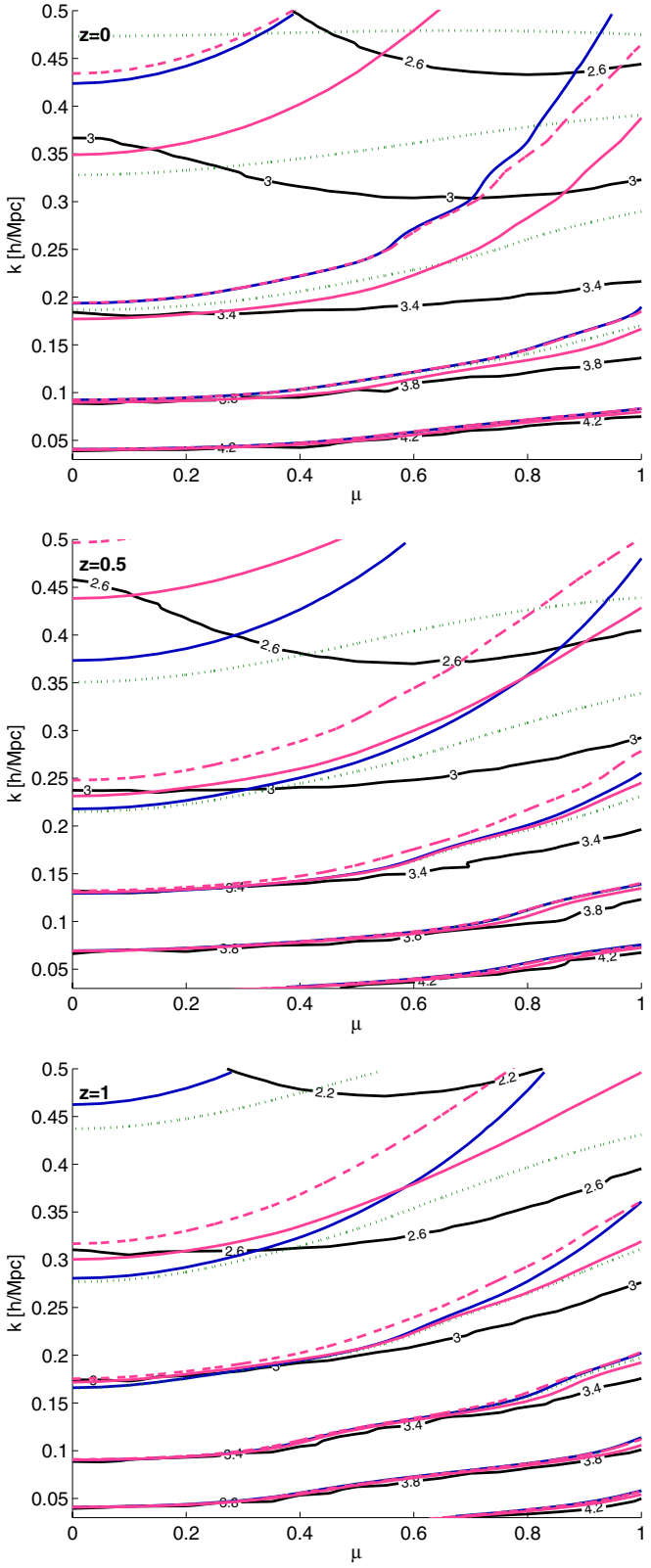

Figure 6. $P^s(k, \mu)$ for $z = 0, 0.5, 1$ as in Figure 2, but using SPT (blue), LPT (dot-dashed green), and Taruya^{++} (solid and dashed pink) treatments of the full redshift space power spectrum, and compared to N-body results (black, labeled). We plot the Taruya^{++} power spectrum with two different methods of evaluating the terms: dashed pink curves correspond to using SPT for $P_{\delta\delta}$, $P_{\delta\theta}$, and $P_{\theta\theta}$ and solid pink curves use the exact N-body power spectra. The SPT curves here do not include any damping terms and the Taruya^{++} curves use a linear theory damping term.

(A color version of this figure is available in the online journal.)

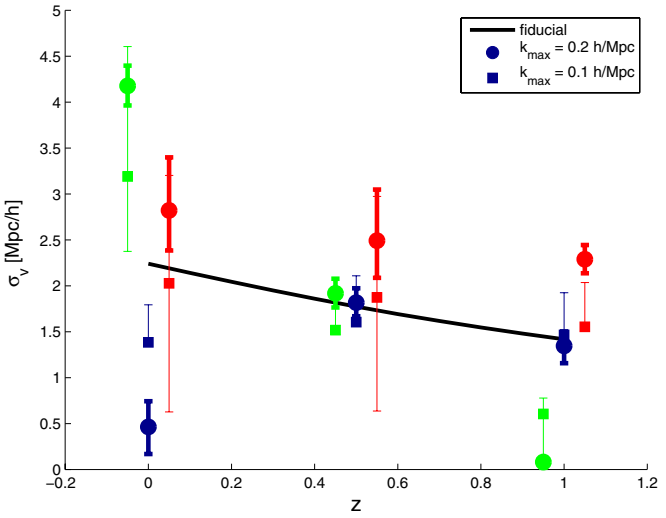

Figure 7. Values of σ_v determined from using empirical damping with the Kaiser limit (blue, centered) and the Scoccimarro formula (red, offset right) and the Taruya^{++} model (light green, offset left) at $z = 0, 0.5, 1$ for $k_{\rm max} = 0.1$ and $0.2\,h$ Mpc^{-1}. For comparison, we have also shown the amount of damping predicted by linear theory (black curve). We have removed the lower error bars for those points whose 1σ limit is consistent with zero.

(A color version of this figure is available in the online journal.)

We emphasize that for the dashed pink curves in Figure 6 (and the results presented in Figure 5) the SPT expansions of $P_{\delta\delta}$, $P_{\delta\theta}$, and $P_{\theta\theta}$ were used instead of the improved PT expressions and this contributes to the deviation between our results and Taruya et al. (2010) who found that their expression provides an unbiased description of the redshift space power spectrum up to $k < 0.205\,h$ Mpc^{-1} at $z = 1$. Yet, a comparison of Figures 4 and 6 reveals that it is the Scoccimarro ansatz that follows the N-body contours more faithfully than the Taruya^{++} model when using the exact nonlinear expressions for $P_{\delta\delta}$, $P_{\delta\theta}$, and $P_{\theta\theta}$ for both models. The solid pink curves in Figure 6 that correspond to the Taruya^{++} model with the real space $P_{\delta\delta}$, $P_{\delta\theta}$, and $P_{\theta\theta}$ measured directly from N-body simulations are especially good near $\mu = 0$ as the Taruya^{++} expression uses an expansion in μ. None of the models, though, get the angular dependence right at lower redshifts.

8. ANGULAR DEPENDENCE AND DAMPING

The damping term in the power spectrum arises from the velocities and also nonlinearities. We first examine the values of σ_v obtained when we allow it to vary as an extra parameter when fitting for the growth rate. We allow for redshift variation between different snapshots but have assumed that σ_v is independent of scale. Figure 7 shows the 1σ constraints on σ_v for the Kaiser, Scoccimarro, and Taruya^{++} models with and without the linear bias (recall that the amount of damping required in LPT is predicted by the model) in comparison to the linear theory prediction shown by the black curve. The bottom error bars have been suppressed where they are consistent with $\sigma_v = 0$.

For many of the models at most of the redshifts, σ_v is not helping to fit the power spectrum shape and so the values are consistent with $\sigma_v = 0$. Only the Scoccimarro model with $k_{\rm max} = 0.1\,h$ Mpc^{-1} is consistent with the linear theory predictions over all the redshifts considered to 1σ. In fact, σ_v in the Taruya^{++} and Kaiser models show a different redshift dependence compared to the fiducial, although it should be exactly degenerate with the linear growth factor $D(z)$ according to the definition below Equation (7). This explains why the

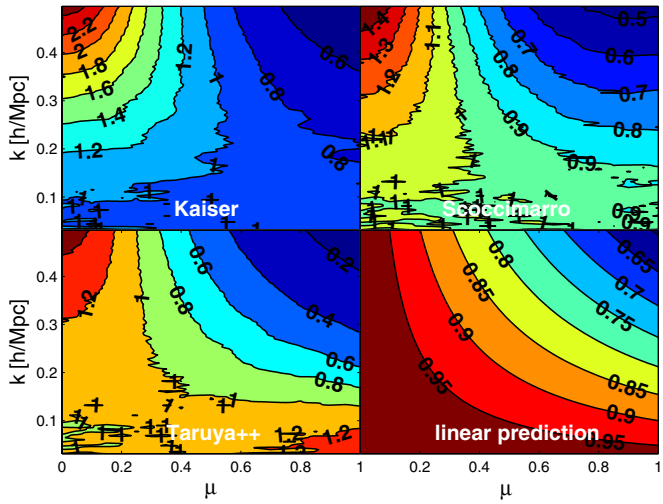

Figure 8. Two-dimensional isocontours of $F(k, \mu)$, using the Kaiser, Scoccimarro, and Taruya^{++} models of the redshift space power spectrum at $z = 0$ using the exact N-body expressions for $P_{\delta\delta}$, $P_{\delta\theta}$, and $P_{\theta\theta}$. The lower right corner shows the prediction of linear theory, i.e., the standard exponential form that is used in the streaming model.

(A color version of this figure is available in the online journal.)

Taruya^{++} power spectrum produces a growth rate that is closest to the fiducial cosmology when σ_v is left as a free parameter; the functional dependence is genuinely distinct from the linear theory as we shall later see.

If the damping term is poorly described by an exponential, then what is the correct functional form that must be applied to these RSD models to reproduce the simulated redshift space power spectrum? Defining the damping term by $F(k, \mu) = P^s_{\rm nbody}(k, \mu)/P^s_{\rm model}(k, \mu)$, we divide the nonlinear redshift space power spectrum as measured in the simulations by the models that we have considered so far. We caution that this function cannot be interpreted as the pairwise velocity PDF for the excellent reasons outlined in Scoccimarro (2004). For physical reasons, it is likely that $F(k, \mu)$ is composed of a series of convolutions of different functions at each scale and the true pairwise velocity PDF is buried in this combination.

Nonetheless it is instructive to characterize the functional form required for these analytic models to succeed in describing the redshift space power spectrum. Figure 8 shows $F(k, \mu)$ for the Kaiser, Scoccimarro, and Taruya^{++} models. For comparison, we have also shown the linear theory prediction for $F(k, \mu)$—the standard exponential in $(fk\mu\sigma_v)^2$—in the lower right corner of Figure 8. A vague similarity between these linear theory curves and those of the Scoccimarro and Taruya^{++} models only begins to appear for $\mu > 0.5$ and $k > 0.2\,h$ Mpc^{-1}. Furthermore, the damping is actually an enhancement for much of the k–μ space, showing amplifications of 50%–150%. As the RSD modeling improves, the maximum amplitudes of $F(k, \mu)$ are smaller, with Scoccimarro and Taruya^{++} models having up to three times smaller deviations. This suggests that we can build on their success by further modeling the nonlinearities and coupling between the density and velocity fields, here through an empirical factor.

Since we are dealing with redshift distortions, $F(k, \mu)$ must enter as a function of $k\mu$, i.e., k_z. We find that the curves of constant k can be described out to $k\mu = 0.5$ by

$$F(k, \mu) = \frac{A}{1 + Bk^2\mu^2} + Ck^2\mu^2, \qquad (15)$$

where A, B, and C are free parameters for each of the models. In general, the parameters are different for each model, but our preliminary investigations suggest that there is some sort of relationship between these values. Expansion of the denominator in $k\mu$ would lead to μ^4 (and higher order) terms, reminiscent of the quartic terms in Tang et al. (2011). In contrast, we find that the amplitude of $F(k, \mu)$ is non-negative on small scales but unity on large scales for $\mu = 0$, as required. The nonlinear, FoG effects are responsible for amplifying the RSD signal perpendicular to the line of sight on small scales, and this is accurately captured by this form. Also noteworthy is the necessity of *three* free parameters—the stretching and squashing effects cannot be simultaneously described with a single parameter as in linear theory damping. If we drop the extra term in C, we find that $F(k, \mu)$ falls off too rapidly to describe regions of large $k\mu$ at small scales. The fitting form agrees with the simulations at the percent level (modulo the small k oscillations discussed below). Although the exact provenance of Equation (15) is the topic of future work, the term in C arises because of extra contributions to the pairwise velocity PDF beyond the usual exponential distribution. Further work is also required to test this functional form at other redshifts, for the moment we have restricted ourselves to considering $z = 0$.

Figure 9 shows that in general $F(k, \mu) = 1$ only when both k and μ are small. In fact, on extremely large scales ($k < 0.05\,h$ Mpc^{-1}), $F(k, \mu) < 1$, but it was not possible to infer the correct form of damping in this regime because the range of $k\mu$ considered is then necessarily small. Of greater concern, however, is that these curves display some oscillatory behavior that raises the issue that incorrect modeling of RSD may contribute to some bias in the baryon acoustic feature. We have confirmed that when $F(k, \mu)$ is kept at a constant value of μ (Figure 9 shows curves of constant k) that the oscillations vary at a level above the sample variance (the latter is no more than 2% on these scales and the oscillations are 6% above the background). Moreover, the shape of the oscillations vary with the RSD model indicating that a genuine bias may be present. This will be explored further in future work, requiring larger simulations.

9. TESTING GRAVITY

We now consider extending the fitting process to include the full set of parameters that can be reasonably constrained by RSD alone, such that $\{\gamma, b, \omega_m, w_0\}$ are now free parameters, but we keep the variation in w fixed at $w_a = 0$. The parameter ω_m is defined in terms of the matter energy density such that $\omega_m = \Omega_m h^2$. We only use the redshift bins at $z = 0.5, 1$ as appropriate for current and future surveys and limit ourselves to using the least biased model of RSD out of each class of models that we have considered. These are the streaming model with nonlinear matter power spectrum, the Scoccimarro formula with SPT power spectra, and the Taruya^{++} model. With the first two, we use linear theory damping; as the previous section showed, the constraints in the Kaiser and Scoccimarro models are fairly insensitive to the value of σ_v used, but we have used an empirical damping term for the Taruya^{++} because this seems to minimize the bias in the derived values for f. We allow the linear bias to vary to soften the constraints as a best-case scenario, since we would expect some covariance between the two in a real galaxy survey. We have also checked that this did not negatively affect the ability of any of these three RSD models to correctly model the growth rate. In all of the models considered, the linear bias is quite tightly constrained and is consistent with $b = 1$ at all

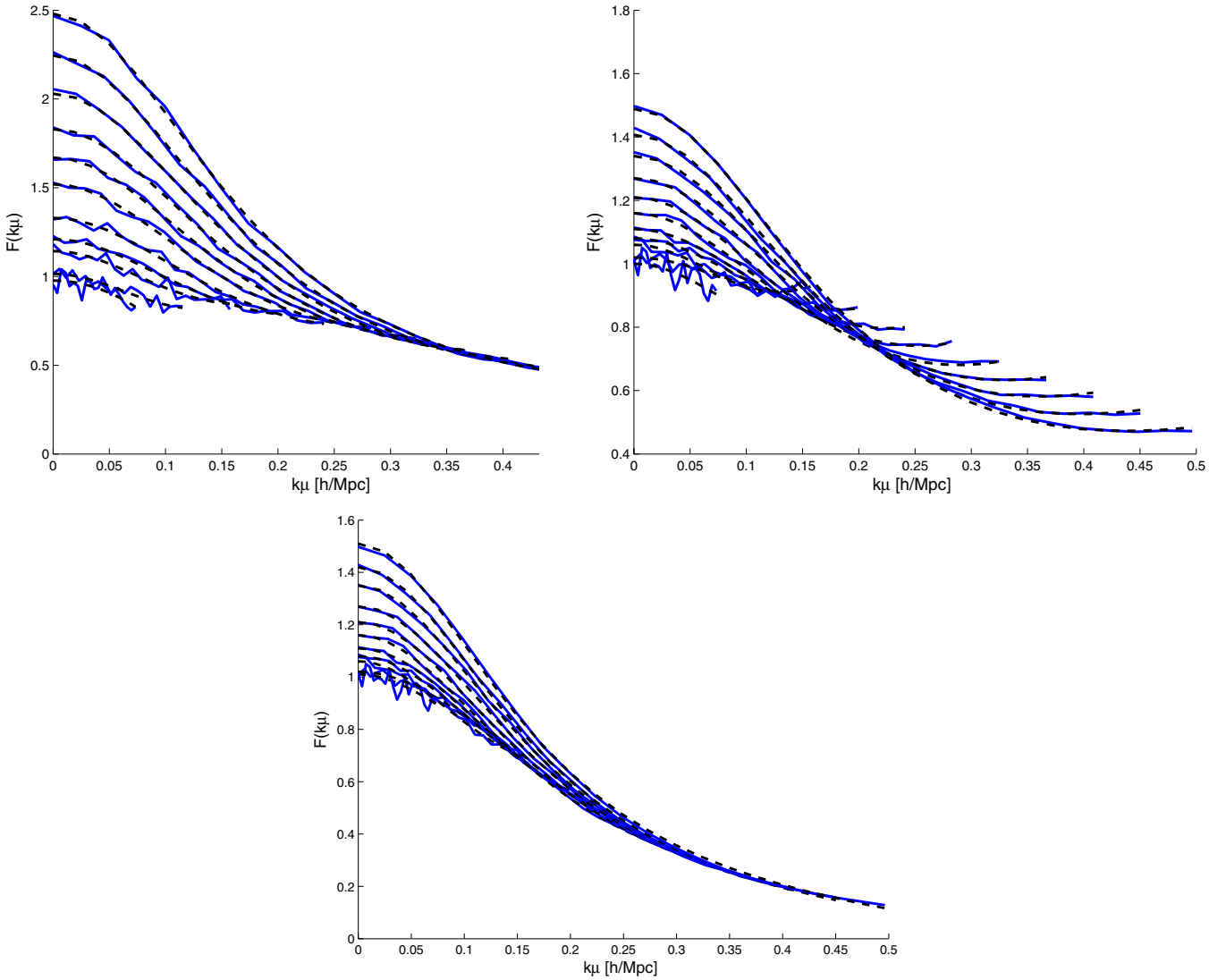

Figure 9. Angular dependence factor $F(k, \mu)$ required for Kaiser (top), Scoccimarro (middle), and Taruya^{++} (bottom) models to exactly describe the redshift space power spectrum at $z = 0$. The blue curves are values of $F(k, \mu)$ as measured directly from simulations and the black dashed lines are the best-fitting curves of the functional form in Equation (15) for a constant value of k, ranging from $0.07 < k < 0.5\,h$ Mpc^{-1}, from bottom curve to top.

(A color version of this figure is available in the online journal.)

redshifts. Furthermore, it is the shape of the redshift space power spectrum, rather than the amplitude, that most informs us about cosmology.

Figure 10 shows the 1σ and 2σ posterior distributions in both the $\gamma - \Omega_m$ (top row) and $\gamma - w_0$ (bottom row) parameter spaces, using out to $k_{\rm max} = 0.1\,h$ Mpc^{-1}. Recall that γ is the gravitational growth index and provides a test of general relativity, which basically predicts $\gamma = 0.55$.

Treating the power spectra measured at $z = 0.5$ and $z = 1$ individually, and restricting to $k < 0.1\,h$ Mpc^{-1}, we found that the joint constraints on γ and Ω_m were mostly unbiased; the posterior distributions of both the Scoccimarro ansatz and Taruya^{++} model contained the fiducial values within their 1σ regions, while for the Kaiser formula the fiducial values were within the 1σ region at $z = 1$ and within the 2σ limit at $z = 0.5$. The contours in the $\gamma - w_0$ plane show similar characteristics, with slightly more bias. The marginalized posterior distributions on γ for both the Scoccimarro and Taruya^{++} models are correct to within 1σ, but these bounds are now generous enough to allow a wide swathe of cosmological models.

The constraints on γ from RSD substantially weaken when using high-redshift slices, as expected from Equation (4) as $\Omega_m(a) \to 1$. The width of the 1σ contours on γ also prevents us from drawing any interesting conclusions about gravity with RSD alone, although in a simplistic sense, the effective volume of the simulations is $\approx$67.5 $[{\rm Gpc}/h]^3$ if we ignore the contributions of larger scale modes. Low-redshift surveys capable of accurately measuring γ, together with accurate modeling of RSD, will be important if we wish to test gravity and cosmology.

One of the advantages of using the gravitational growth index is that we expect to measure the same value of γ at each redshift for scale-independent theories of gravity and we may combine observations from several redshift bins to strengthen our constraints. We have combined the power spectra in these redshift bins, neglecting any covariance between them. This gives the purple contours seen in Figure 10. But none of the models have benefited from such treatment, despite the substantial improvement in the statistical error. This is partly because it would be preferable to fit each redshift slice individually since the sensitivity of the results to $k_{\rm max}$ is different

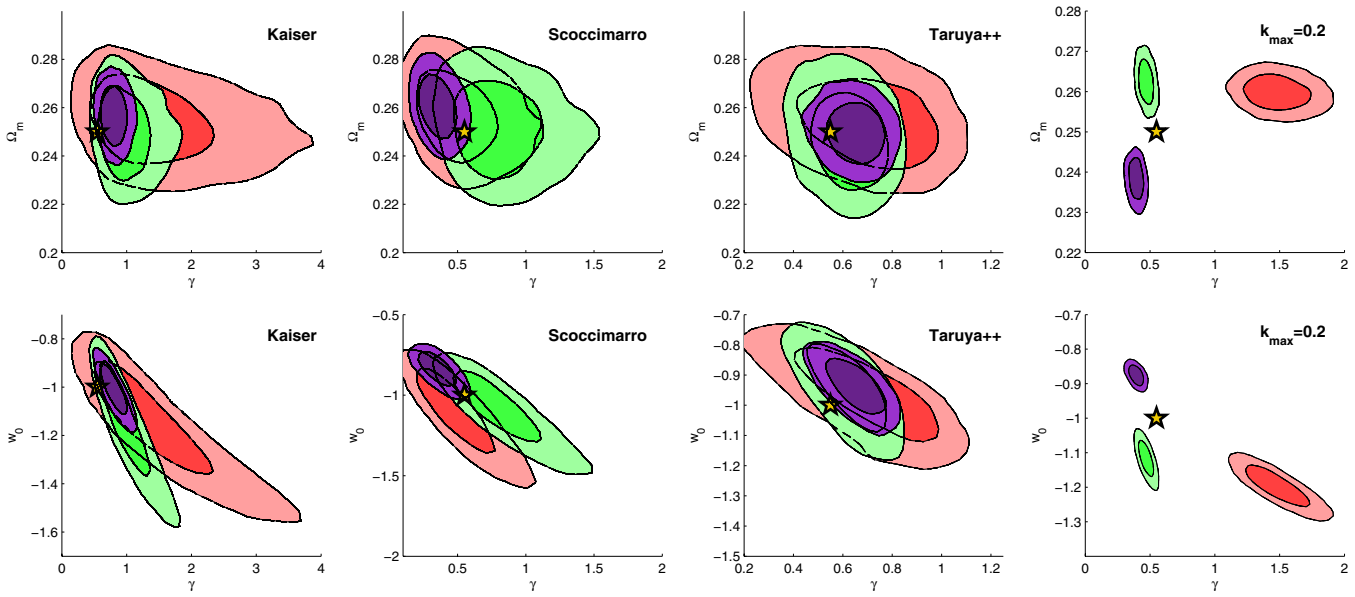

Figure 10. 1σ and 2σ posterior distributions on γ after extending the parameter set to include $\{\gamma, b, \omega_m, w_0\}$ for the streaming model (leftmost column), the Scoccimarro model (second column), and the Taruya^{++} model (third column) for $k < 0.1\,h$ Mpc^{-1}. In each of these figures, the posteriors are colored according to redshift, $z = 0.5$ (light green), $z = 1$ (red) and joint fits over both redshifts are in dark purple. Note the change in scales between the figures. The rightmost column shows the Kaiser (red), Scoccimarro (light green), and Taruya^{++} (dark purple) models using $k < 0.2\,h$ Mpc^{-1} at $z = 1$. The fiducial parameters are marked with a star. (A color version of this figure is available in the online journal.)

at each redshift, but also indicates that some of these models are becoming less valid as the redshift distribution becomes more nonlinear. This is particularly true for the Scoccimarro ansatz, whose joint posteriors are the most inconsistent with the two individual distributions.

Attempting to use power spectrum information out to $k_{\rm max} = 0.2\,h$ Mpc^{-1} with any of these models severely exacerbates the bias, even as the statistical errors shrink. For example, the rightmost column of Figure 10 shows that at $z = 1$ where the redshift space density field might be expected to be reasonably linear, the posterior distributions are far more than 2σ away from their fiducial values regardless of the model. However, the Taruya^{++} model could certainly benefit from using a different estimate of $P_{\delta\delta}$, $P_{\delta\theta}$, and $P_{\theta\theta}$ on small scales.

10. CONCLUSIONS

With an combined volume of 67.5 $[{\rm Gpc}/h]^3$, we have tested the robustness of the Kaiser limit, Scoccimarro ansatz, Lagrangian, and standard perturbation theories and Taruya^{++} models of RSDs, with a number of variations on the form of the damping term. Of all the linear, quasi-linear, and nonlinear models for the redshift space power spectrum that we have considered, we found that the least biased of these for determining the growth rate f was the model proposed by Taruya et al. (2010) based on the Taruya^{++} model if we use SPT to evaluate the real space components and restrict the scales used to $k < 0.1\,h$ Mpc^{-1}. However, none of the models delivered accurate results if we extend them to $k = 0.2\,h$ Mpc^{-1}.

Even with sophisticated perturbation theory schemes, all the models that we have considered fail to describe correctly the angular dependence of the redshift space power spectrum in the quasi-linear regime and mischaracterize the nonlinear FoG effects. Instead, we present a fitting formula for the angular dependence factor that, in comparison to simulations, accounts accurately for both damping and FoG effects. Further work is needed to relate this to underlying theory and to test its universality. One issue of concern is the possible interaction of the RSD modeling with extraction of the true BAO scale.

The simulations provide the redshift space power spectrum of the dark matter halos. As work such as Okumura & Jing (2011) shows, the behavior of galaxies relative to dark matter can have added complications. We cannot fully account for the difference between what is measured in a galaxy survey and models of RSDs until we also consider the problems of biased tracers, as well as wide angle RSDs within perturbation theory and additional astrophysical effects such as non-zero neutrino masses. Other areas of interest include using RSDs to constrain the metric potentials, instead of the gravitational growth index, to probe the gravitational model.

In terms of testing gravity from the growth rate, we found that the results are not robust with respect to inaccurate RSD modeling. Bias in the confidence regions for the gravitational growth index γ and other cosmological parameters can be appreciable, making it dangerous to use modes as large as $k = 0.1\,h$ Mpc^{-1}, even for a rather conservative set of cosmological parameters. In fact, the set $\{f, b, \Omega_m, w_0\}$, is substantially smaller than those cosmological parameters that must be considered (Simpson & Peacock 2010) if we are to rule out general relativity with any confidence.

This might be ameliorated by combination of RSD with other probes, though there is also the danger that this will merely reduce the statistical errors. If the bias in the RSD results is particularly strong, as is the case with $k_{\rm max} = 0.2\,h$ Mpc^{-1}, there is the additional risk that the RSD data set will simply be inconsistent with and pull the results of other measurements or that the resultant distribution will be multimodal. Including the parameters from our angular dependence factor, or its future forms, may provide a robust approach to mapping growth and gravity with RSDs.

J.K. thanks the Berkeley Lab and the Berkeley Center for Cosmological Physics, the Los Alamos National Laboratory, the Institute of Astronomy, the Cambridge and Swinburne

University of Technology for hospitality while this work was conducted. J.K. also thanks Chris Blake for helpful comments on a draft of this article. This work has been supported in part by the Director, Office of Science, Office of High Energy Physics, of the U.S. Department of Energy under the contract No. DE-AC02-05CH11231, and the World Class University grant R32-2009-000-10130-0 through the National Research Foundation, Ministry of Education, Science and Technology of Korea. J.K. and G.F.L. acknowledge support from ARC Discovery Project DP0665574 and significant computational resources through the INTERSECT/NCI partner share.

REFERENCES

Abazajian, K. N., Adelman-McCarthy, J. K., Ageros, M. A., et al. 2009, ApJS, 182, 543
Bhattacharya, S. 2011, Phys. Rev. D, 83, 043004
Blake, C., Brough, S., Colless, M., et al. 2011, MNRAS, 415, 2876
Carlson, J., White, M., & Padmanabhan, N. 2009, Phys. Rev. D, 80, 043531
Carroll, S. M. 2001, Living Rev. Rel., 4, 9
Cole, S., Percival, W. J., Peacock, J. A., et al. 2005, MNRAS, 362, 505
Desjacques, V., & Sheth, R. K. 2010, Phys. Rev. D, 81, 023526
Drinkwater, M. J., Jurek, R. J., Blake, C., et al. 2010, MNRAS, 401, 1429
Dvali, G., Gabadadze, G., & Porrati, M. 2000, Phys. Lett. B, 485, 208
Eisenstein, D., Weinberg, D. H., Agol, E., et al. 2011, ApJ, 142, 72
Fang, W., Hu, W., & Lewis, A. 2008, Phys. Rev. D, 78, 087303
Fisher, K. B. 1995, ApJ, 448, 494
Guzzo, L., Pierleoni, M., Meneux, B., et al. 2008, Nature, 451, 541G
Hawkins, E., Maddox, S., Cole, S., et al. 2003, MNRAS, 346, 78
Heavens, A. F., Matarrese, S., & Verde, L. 1998, MNRAS, 301, 797
Heitmann, K., White, M., Wagner, C., Habib, S., & Higdon, D. 2010, ApJ, 715, 104
Jackson, J. C. 1972, MNRAS, 156, 1P
Jain, B., & Bertschinger, E. 1994, ApJ, 431, 495
Jennings, E., Baugh, C. M., & Pascoli, S. 2011a, MNRAS, 410, 2081
Jennings, E., Baugh, C. M., & Pascoli, S. 2011b, ApJ, 727, L9
Jing, Y. P. 2005, ApJ, 620, 559
Kaiser, N. 1987, MNRAS, 227, 1
Laureijs, R. 2009, (arXiv:0912.0914)
Lawrence, E., Heitmann, K., White, M., et al. 2010, ApJ, 713, 1322
Le Févre, O., Vettolani, G., Garilli, B., et al. 2005, A&A, 439, 845
Lewis, A., & Bridle, S. 2002, Phys. Rev. D, 66, 103511
Lewis, A., Challinor, A., & Lasenby, A. 2000, ApJ, 538, 473
Linder, E. V. 2005, Phys. Rev. D, 72, 043529
Linder, E. V. 2008, Astropart. Phys., 29, 336
Matsubara, T. 2008, Phys. Rev. D, 77, 063530
Okumura, T., & Jing, Y. P. 2011, ApJ, 726, 5
Park, C., Vogeley, M. S., Geller, M. J., & Huchra, J. 1994, ApJ, 431, 569
Peacock, J. A., & Dodds, S. J. 1994, MNRAS, 267, 1020
Peebles, P. J. E. 1976, Ap&SS, 45, 3
Percival, W. J., & White, M. 2009, MNRAS, 393, 297
Samushia, L., Percival, W. J., & Raccanelli, A. 2011, (arXiv:1102.1014)
Sargent, W. L. W., & Turner, E. L. 1977, ApJ, 212, L3
Schlegel, D. J., Bebek, C., Heetderks, H., et al. 2009, (arXiv:0904.0468)
Scoccimarro, R. 2004, Phys. Rev. D, 70, 083007
Scoccimarro, R., Couchman, H. M. P., & Frieman, J. A. 1999, ApJ, 517, 531
Simpson, F., & Peacock, J. A. 2010, Phys. Rev. D, 81, 043512
Smith, R. E., Peacock, J. A., Jenkins, A., et al. 2003, MNRAS, 341, 1311
Springel, V. 2005, MNRAS, 364, 1105
Suto, Y. 2010, Proc. SPIE, 7733, 773302
Tang, J., Kayo, I., & Takada, M. 2011, MNRAS, 416, 2291
Taruya, A., Nishimichi, T., & Saito, S. 2010, Phys. Rev. D, 82, 063522
Tocchini-Valentini, D., Barnard, M., Bennett, C. L., & Szalay, A. S. 2011, (arXiv:1101.2608)
Zel'dovich, Ya. B. 1970, A&A, 5, 84